Journal of Polymer Research (2021) 28: 119
https://doi.org/10.1007/s10965-021-02463-8

ORIGINAL PAPER

Covalent triazine based polymer with high nitrogen levels for removal of copper (II) ions from aqueous solutions

Mohammad Dinari[1] · **Nazanin Mokhtari**[1] · **Mohammad Hatami**[1]

Received: 4 December 2020 / Revised: 11 February 2021 / Accepted: 18 February 2021/ Published online: 13 March 2021

Abstract

The tremendous popularity of porous organic polymers in all fields of Science is irrefutable these days. The current study investigates the application of an accessible covalent triazine-based polymer (CTP) synthesized from 2,4,6-tris(hydrazino)-1,3,5-triazine (THT) and terephthaldehyde (TA) in a Pyrex sealed tube. The prepared CTP can efficiently remove the $Cu^{(II)}$ ions from aqueous solutions. After the successful CTP synthesis, it was characterized using different methods, including FE-SEM, XRD, CO_2 adsorption isotherm, and TGA. A wide range of pH with different adsorbate concentrations and times were investigated to study the batch adsorption experiment. The excellent adsorption of $Cu^{(II)}$ ions at the optimal pH of 7 with a maximum capacity of 86.95 mg. g^{-1} and excellent thermal stability makes it the right industrial investigation choice. Moreover, the obtained data reveal that the adsorption isotherm obeys the Langmuir model, and the adsorption kinetics obeys the pseudo-second-order model.

Keywords Porous organic polymers · Covalent triazine-based polymer · Adsorption · Copper

Introduction

In recent years, water pollution and the shortage of water sources have become significant concerns [1–4]. The most severe threats to water sources are heavy metals regarding their persistency in nature, bio-accumulation tendency, and toxicity [5, 6]. During the past years, different removal methods have been developed for heavy metals, including electrolysis [7], filtration [8], reduction [9], precipitation [10], and adsorption [11–14]. The simplicity, as well as the efficiency, made adsorption one of the most reliable methods [15]. Mercury, zinc, chromium, nickel, arsenic, copper, cadmium, and lead are known as the most harmful heavy metals existing in water sources [16, 17]. Copper is one of those toxic heavy metals widely used in various industries including, paint and pigment, mining, fertilizer, electroplating, and metal finishing industries [18]. The rapid industrial development caused the accumulation of a large amount of copper into the environment [19]. Heavy metals are non-biodegradable, making them existing in nature for long times [20]. Going beyond the limiting tolerance of Cu(II) ions in water and wastewater would cause serious health problems. Therefore, removing Cu(II) ions from industrial wastewater is necessary [21]. In recent years, considerable attention has been concentrated on designing effective and low-cost methods for the adsorption of Cu(II) ions from Cu (II)-rich effluents [19].

Various materials have been used in water treatment as the adsorbents such as polymers [22], clays [23], metal oxides [24], carbon aerogel [25], and activated carbons [26]. The lack of chemical bonds to metal ions in these traditional adsorbents decreased their metal removal performance [27]. Thus, finding new materials acting as effective adsorbents is of significant interest. Lack of enough active surface sites, diffusion limitation, high cost, as well as, separation and regeneration difficulties caused unsatisfactory results for most of these adsorbents. Developing new structures with easy recovery, high adsorption capacity, low diffusion resistance, and large surface area is a long-lasting challenge in green chemistry. Considering the mentioned properties, covalent triazine polymer (CTPs) are gaining vital interests in heavy metal removal from aqueous solutions [28, 29].

Porous organic polymers (POPs) are a fascinating class of porous materials made of organic molecules connecting

✉ Mohammad Dinari
dinari@iut.ac.ir; mdinary@gmail.com

[1] Department of Chemistry, Isfahan University of Technology, 84156-83111 Isfahan, I.R. Iran

via strong covalent bonds. Regarding their unique properties, such as a variety of structures, well-defined porosities, and high surface areas, POPs found diverse applications in different branches of science [30, 31]. The ability to use various chemical functionalities in their structure makes them become designable and task-specific materials. Among the different classes of POPs, CTPs have gained interest in the synthesis of organic nanostructures [32]. Metal-organic frameworks (MOFs) have common properties to CTPs, such as high specific surface area. However, the superiority of the CTPs can be explained as the chemical stability in acidic solutions [33–37].

CTPs are materials with nitrogen-rich porous frameworks with surface basicity and large surface area [38]. The presence of C-N-C six-membered rings caused CTPs to have broad applications in gas storage [38], sensing [28], catalysis [39], and water treatment, especially in the removal of heavy metals [28, 29]. Tunable surface essential functions, large pore volume, high surface area, as well as high thermal and chemical stability made CTPs excellent materials for metal removal [28, 29].

The present study introduced a hydrazone-based CTP as a suitable adsorbent to remove Cu(II) ions from aqueous solutions. Using available and cost-efficient materials (hydrazine, terephthaldehyde, and 2,4,6-trichloro-1,3,5-triazine) and a simple preparation method made it a good model of industrialization.

Experimental details

Materials

All the chemicals were purchased from Sigma Aldrich and Merck chemical companies and used without further purification.

Synthesis of *2,4,6-tris(hydrazino)-1,3,5-triazine (THT)*

A modified procedure from the literature was used to prepare THT [40]. In a typical procedure, a solution of 0.552 g of 2,4,6-trichloro-1,3,5-triazine (TCT) in 5 mL of 1,4-dioxane was prepared and slowly added to a solution of 18 mmol of hydrazine hydrate (HZ) in 5 mL of 1,4-dioxane for 1 h. The mixture stirred for 2 h at room temperature. In the end, the precipitated product was filtered and washed with distilled water and 1,4-dioxane severally, then dried at 70°C under vacuum for 12 h (yield: 80 %). Elemental analysis (experimental/ theoretical): C: 19.75/ 21.05 ;H: 6.02/ 5.30 ;N: 70.94/ 73.65.

Synthesis of porous N-riched CTP (THT-TA-CTP)

To prepare THT-TA-CTP, a pyrex tube charged with THT (0.64 mmol), terephthaldehyde (TA) (0.96 mmol), mesitylene (1.0 mL), 1,4-dioxane (1.0 mL), and 100 µL aqueous acetic acid (6 M). Then it was sonicated for 5 min, vacuumed, flame sealed, and heated to 120°C for 72 h. The yellow precipitated product separated by centrifugation, washed with chloroform (5 mL), THF (5 mL), and acetone (5 mL), respectively. The product was then purified using a Soxhlet extractor to remove all the oligomers from the structure. Finally, the product was vacuum dried at 70°C.

Characterization

The X-ray diffraction (XRD) patterns were recorded on a Bruker (Advanced D8 Bruker AXS, Berlin, Germany) using Cu Kα in the range of 2–80°. The field-emission scanning electron microscopy (FESEM) images were recorded on a HITACHI (S-4160, Tokyo, Japan) device for studying the surface morphology of the THT-TA-CTP structure. A JASCO FT-IR (680 plus, Tokyo, Japan) impact spectrometer was used to obtain Fourier transform infrared (FT-IR) spectra for studying the functional groups presented in the THT-TA-CTP structure. The thermal stability of the THT-TA-CTP was investigated with the thermal gravimetric analysis (TGA) on an STA (503, Hüllhorst, Germany) device. The samples were heated to 800°C with a ramp of 10°C/min. The surface porosity parameters were investigated by CO_2 adsorption isotherm, which is recorded on a MicroActive TriStar II plus 2.03 (Micrometrics, USA). The concentration of $Cu^{(II)}$ ions was studied with a Flame atomic adsorption spectrophotometer (FAAS; PerkinElmer 2380-Waltham) equipped with a Cu (II) hollow cathode lamp.

Batch adsorption experiment: kinetic and isotherm investigation

The THT-TA-CTP ability in the adsorption of metal ions was studied using $Cu^{(II)}$ metal ions. An appropriate amount of copper nitrate trihydrate was dissolved in distilled water to prepare a stock solution of 100 mg. L^{-1} $Cu^{(II)}$ ions. A 50 mL polyethylene bottle was charged with 10 mg of adsorbent and 25 mL of 10 mg. L^{-1} solution of $Cu^{(II)}$ ions. The universal buffer was used to adjust the pH in the range of 2–12. Then, the bottles were shaken at 174 rpm at room temperature for 240 min. Afterward, the solutions were centrifuged to remove the adsorbent, and the concentration of $Cu^{(II)}$ ions was evaluated using FAAS techniques.

Moreover, polyethylene bottles containing solutions with concentration ranged (2-150 mg. L^{-1}) was charged with 10 mg of the adsorbent at the optimized condition, were used to investigate the adsorption isotherm.

Regarding the FAAS data, the adsorption capacity (q_e) and the removal efficiency (R_e) determined from the following equations (Eqs. 1 and 2):

$$R_e = \left[\frac{(C_i - C_e)}{C_i}\right] \times 100 \quad (1)$$

$$q_e = \frac{V}{m}(C_i - C_e) \quad (2)$$

In these equations, C_i (mg. L^{-1}), C_e (mg. L^{-1}), V (L), and m (g) is the initial concentration of $Cu^{(II)}$ ions, the final equilibrium concentration of $Cu^{(II)}$ ions, volume of the solutions, and the mass of adsorbent, respectively [41].

To investigate the kinetics of the adsorption reaction, 25 mL of 80 mg. L^{-1} solution of $Cu^{(II)}$ was prepared and charged with 10 mg of the adsorbent at pH = 7 as the optimized pH. The solutions were shaken for 20–180 min. Finally, the mixtures were centrifuged to remove the adsorbent, and the supernatant was analyzed with the FAAS device.

Results and discussion

Characterizations

The overall synthesis procedure of THT-TA-CTP was illustrated in scheme 1. The substitution of chlorine atoms with hydrazine in an S_N2 like mechanism led to the formation of THT. Then, THT-TA-CTP was prepared with the reaction with TA in a sealed pyrex tube. The presence of nitrogen atoms in the structure increased heavy metal removal via a pincer type complexation to the metal center.

Functional group changes were identified using FT-IR spectroscopy (Fig. 1). The FT-IR spectra of THT, TA, and their corresponding CTP were shown in Fig. 1. The primary vibrations of TA are the aldehyde C-H bond stretching and the aldehyde carbonyl group, which are appeared at 2756–2864 cm^{-1} and 1694 cm^{-1} (Fig. 1b), respectively. Besides, in the THT spectrum, the bands at 3279–3312 cm^{-1} and 2924 cm^{-1} are corresponding to the $–NH_2$ and –NH– bonds vibration, respectively [42]. Also, the main stretching modes of the s-triazine ring were observed at 1541–1567 cm^{-1} (Fig. 1c). In the case of THT-TA-CTP, the carbonyl band of the TA at 1694 cm^{-1} was disappeared due to the completion of the reaction with THT. More importantly, the formation of new –C=N– bonds at 1619 cm^{-1} proves the formation of THT-TA-CTP (Fig. 1a).

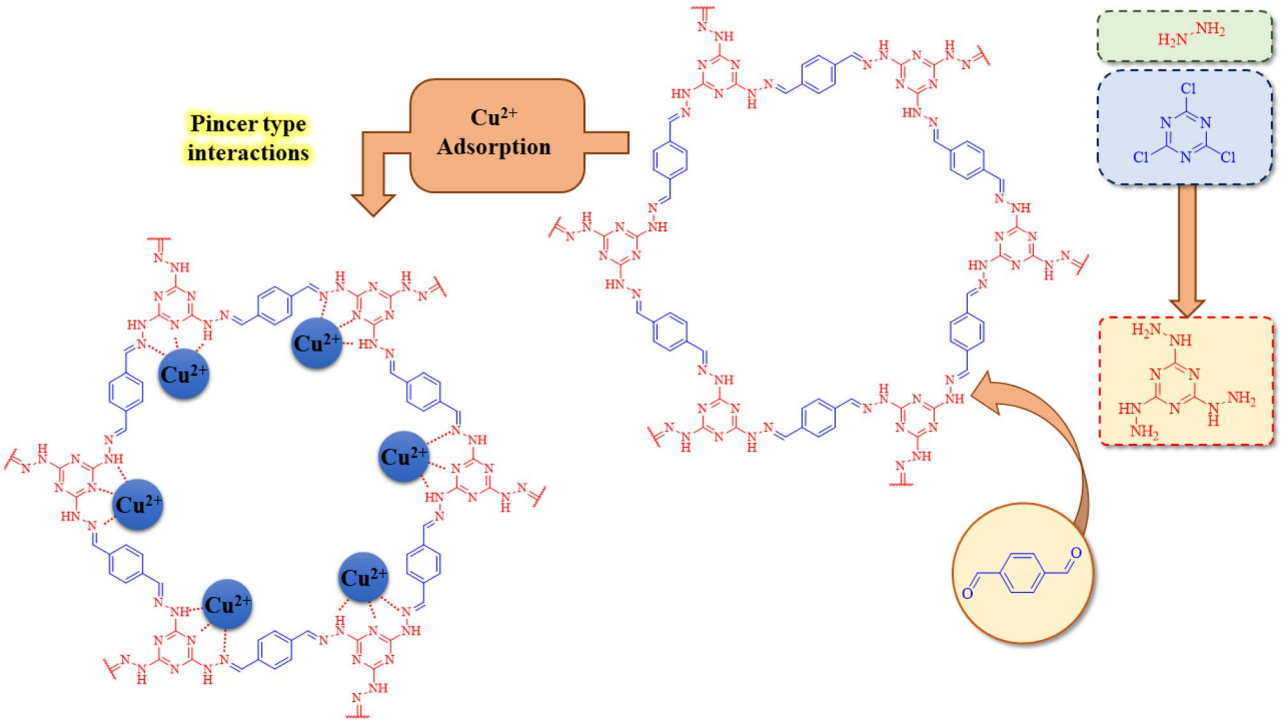

Scheme 1 Schematic illustration of THT-TA-CTP preparation and $Cu^{(II)}$ removal

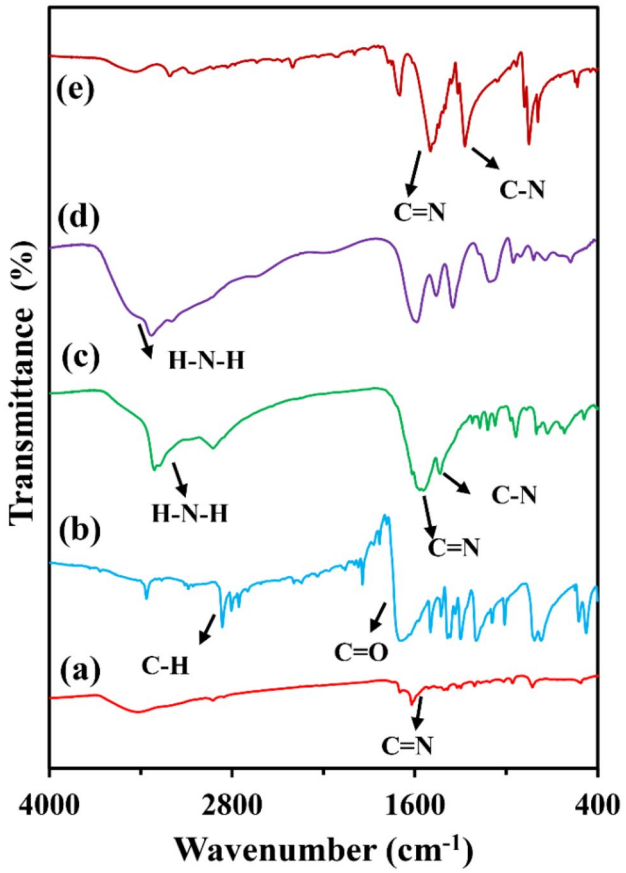

Fig. 1 FT-IR spectra of (**a**) THT-TA-CTP, (**b**) TA, (**c**) THT, (**d**) hydrazine, and (**e**) TCT

To investigate the crystallinity of the THT-TA-CTP, its XRD pattern were recorded (Fig. 2). The pattern shows the semi-crystalline nature of the THT-TA-CTP. The bands observed at 15–35°, especially those at 18.5° and 25.3° are related to the π- π stacking interactions presented between the THT-TA-CTP layers [43, 44]. Also, the crystal size

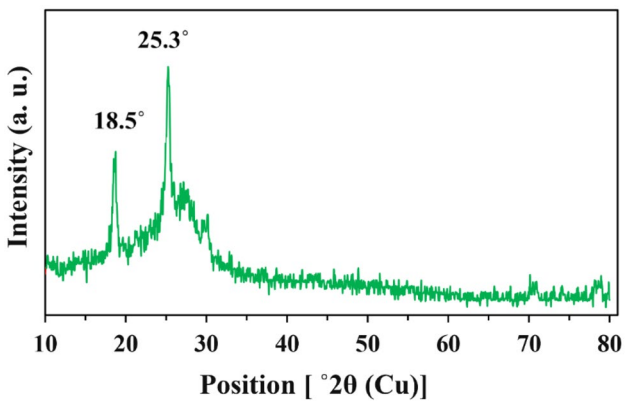

Fig. 2 XRD pattern of THT-TA-CTP

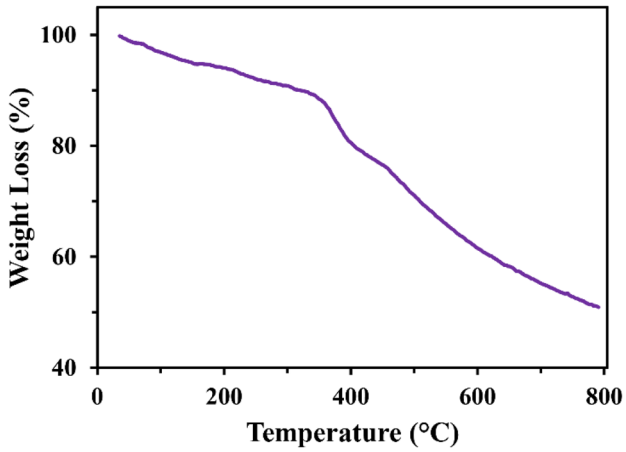

Fig. 3 TGA pattern of THT-TA-CTP

was determined with the Scherrer equation. The crystal size was found to be 28.82 nm from the peak presented at 25.3°.

The thermal stability of the THT-TA-CTP was studied using TGA. The obtained data, including the decomposition temperature of 5 % wt. ($T_{5\%}$), the decomposition temperature of 10 % wt. ($T_{10\%}$), and char yield was found to be 160°C, 320°C, and 50 %, respectively (Fig. 3). The limiting oxygen index (LOI) for halogen-free compounds can be calculated through the Van Krevelen and Hoftyzer equation [45]. LOI was found to be 37, which is a sign of being a self-extinguishing material corroborating the high thermal stability of the THT-TA-CTP (Fig. 3).

The surface porosity parameters of the THT-TA-CTP were studied using the CO_2 adsorption isotherm. Using CO_2 instead of N_2 is a standard method for microporous materials. The specific surface area of the BET isotherm of CO_2 adsorption (Fig. 4) was found to be 100.79 $m^2\ g^{-1}$. The

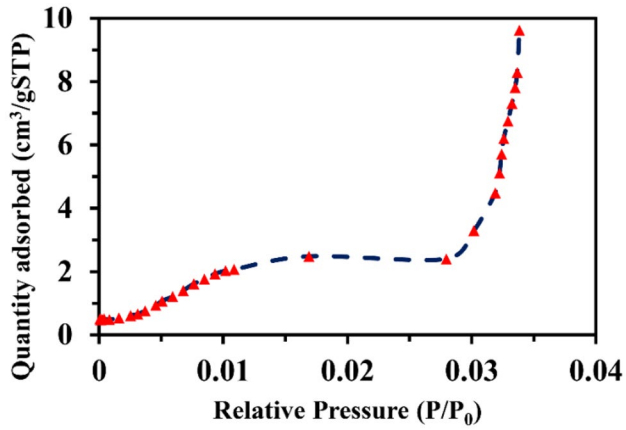

Fig. 4 CO_2 adsorption isotherm of THT-TA-CTP

mean pore diameter and total pore volume were also found to be 0.5 nm and 0.03 $cm^3\ g^{-1}$ using the Horvath-Kawazoe method [46].

For the next investigation, the surface morphology of the THT-TA-CTP was studied using FE-SEM images. These images revealed a stable spongy, porous structure for THT-TA-CTP (Fig. 5).

Effects of pH on the performance of adsorption

To study the effect of pH on the adsorption experiment, the universal buffer in the range of 2–12 was used. The concentration of the remained $Cu^{(II)}$ ions in the solutions after the equilibrium was studied using FAAS. The removal efficiency of $Cu^{(II)}$ ions from 10 mg. L^{-1} solutions in different pH are explored and shown in Fig. 6 (Eqs. 1 and 2). The adsorption is not efficient in acidic pH values, which might be related to the deactivation of active nitrogen sites in the presence of acidic protons. Also, pH values above 7 can induce the precipitation of $Cu^{(II)}$ ions as the hydroxide, which is not satisfactory; thus, the pH of 7 selected as the optimal pH to reach the highest removal efficiency (Fig. 6).

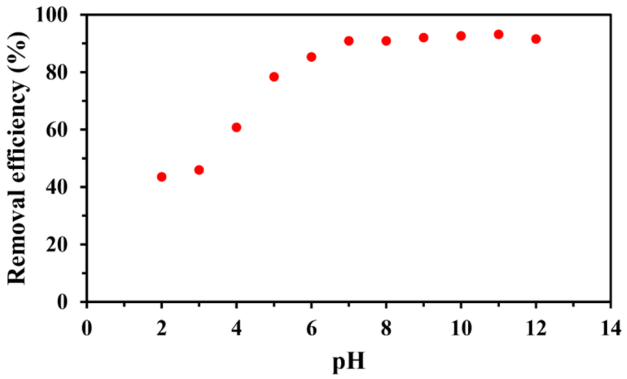

Fig. 6 The effects of the pH of the solution on the Cu(II) removal

Isotherms and the kinetic equation for adsorption equilibrium values of adsorption

Isotherm equations

The adsorbent characteristics, including the equilibrium values of adsorption and the maximum amount of $Cu^{(II)}$ ions (mg) adsorbed per adsorbent mass unit (g), can be calculated by fitting the adsorption data into the Langmuir, Freundlich, Tempkin, and Dubinin-Radushkevich isotherm models. The monolayer adsorption of $Cu^{(II)}$ ions on the external surface of THT-TA-CTP was studied using the Langmuir isotherm equation (Eq. 3) [47]

$$\frac{1}{q_e} = \left(\frac{1}{K_L q_m}\right)\frac{1}{C_e} + \frac{1}{q_m} \tag{3}$$

.

In this equation, K_L (L. mg^{-1}) is the Langmuir isotherm constant, q_m (mg. g^{-1}) is maximum monolayer coverage capacity, q_e (mg. g^{-1}) is the amount of metal adsorbed at equilibrium, and C_e (mg. L^{-1}) is the equilibrium concentration of the $Cu^{(II)}$.

The heterogeneous surface characteristics can be described with the Freundlich isotherm (Eq. 4) [48].

$$\ln q_e = lnK_F + \frac{1}{n}\ln C_e \tag{4}$$

where K_F is the Freundlich isotherm constant, n is the adsorption intensity, q_e (mg. g^{-1}) is the amount of metal

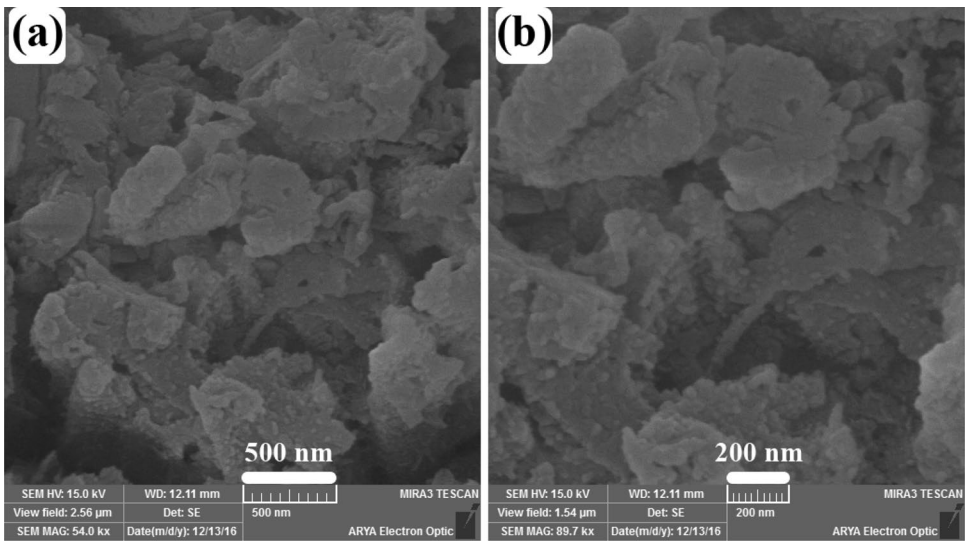

Fig. 5 FE-SEM images of THT-TA-CTP

adsorbed at equilibrium, and C_e (mg. L^{-1}) is the equilibrium concentration of the $Cu^{(II)}$.

The interaction between the $Cu^{(II)}$ ions and the THT-TA-CTP was explored by ignoring the too high or too low concentration with the Temkin isotherm (Eq. 5) [49, 50]. The adsorption heat of all molecules is linearly reduced and can be calculated from this equation.

$$q_e = \frac{RT}{b_T}\ln A_T + \frac{RT}{b_T}\ln C_e \tag{5}$$

in the above equation, R (8.314 J. mol^{-1}. K^{-1}) is the universal gas constant, T is the temperature (here 298 K), b_T is the Temkin isotherm constant, A_T (L. g^{-1}) is the Temkin isotherm equilibrium binding constant, q_e (mg. g^{-1}) is the amount of metal adsorbed at equilibrium, and C_e (mg. L^{-1}) is the equilibrium concentration of the $Cu^{(II)}$.

The adsorption mechanism was investigated with the Dubinin-Radushkevich (Eq. 6) [47] isotherm equation using the Gaussian energy distribution on the surface of THT-TA-CTP.

$$lnq_e = lnq_s - K_{ad}.\epsilon^2 \tag{6}$$

In this equation, ε is the Dubinin – Radushkevich isotherm constant, K_{ad} (mol^2. kJ^{-2}) is the adsorption equilibrium constant, q_s (mg. g^{-1}) is the theoretical isotherm saturation capacity, and q_e (mg. g^{-1}) is the amount of metal adsorbed at equilibrium.

These isotherms were studied, and their results are summarized in Table 1. By comparing the R^2 values, it was found that the Langmuir model was best fitted to the adsorption data. The q_m value shows the maximum adsorption capacity of THT-TA-CTP and found to be 86.95 mg. g^{-1}. The spontaneity of the reaction was investigated by studying the R_L value. The R_L value of the adsorption found to be 0.3–0.7, revealing the fact that the adsorption was spontaneous.

Kinetic investigation

The adsorption kinetics were explored based on the Lagergren equations [51]:

Pseudo-first order:

$$\ln(q_e - q_t) = \ln q_e - k_1 t \tag{7}$$

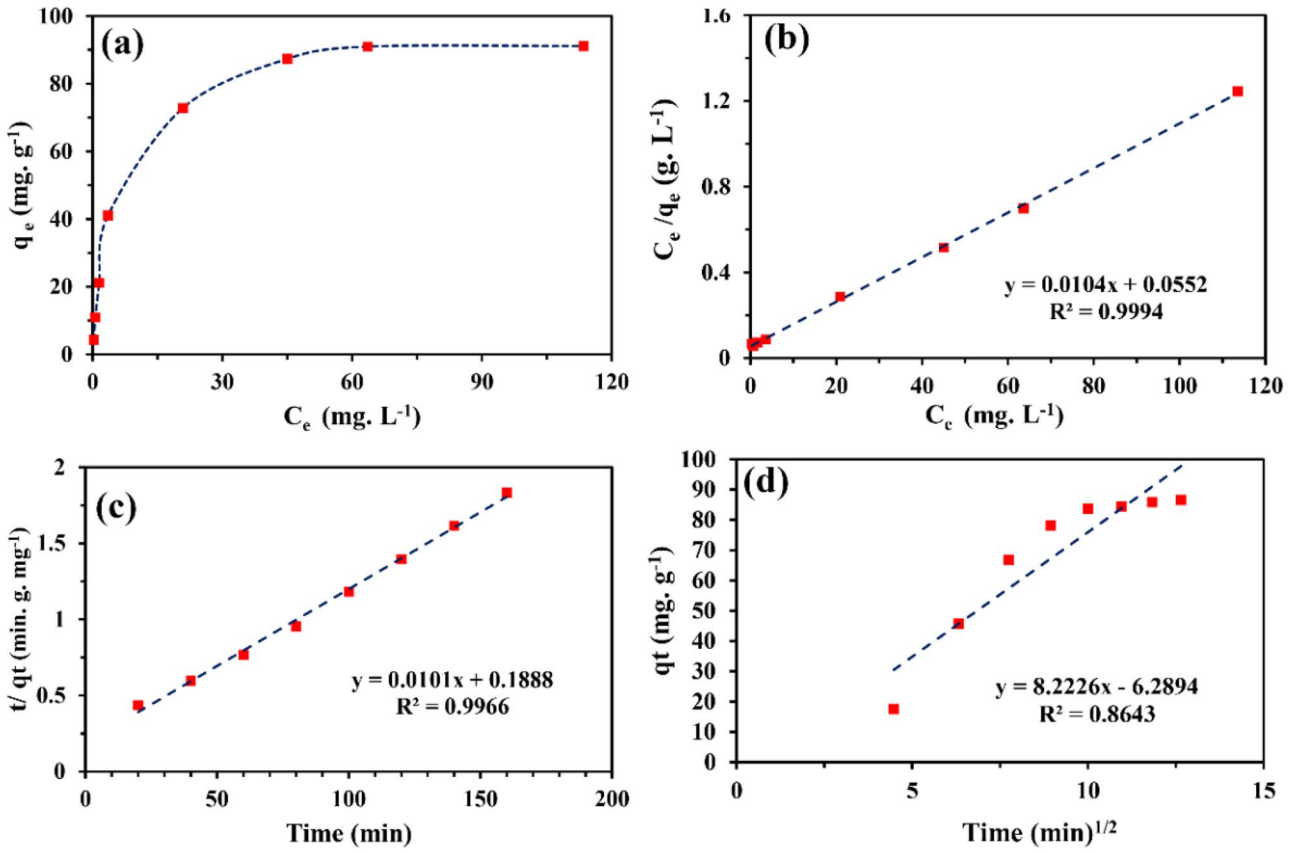

Fig. 7 (**a**) Adsorption isotherm for $Cu^{(II)}$ removal at optimal condition, (**b**) Langmuir plot of adsorption, (**c**) pseudo-second-order kinetic model, and (**d**) Intra-particle diffusion model

Table 1 Isotherms and Kinetic coefficients for Cu(II) removal using Eqs. 3–9

Isotherms coefficients													
Model	Langmuir			Freundlich			Temkin			Dubinin-Radushkevich			
Adsorbate	q_m	K_L	R^2	K_F	N	R^2	K_T	b_T	R^2	q_s	K_{ad}	R^2	
$Cu^{(II)}$ ions	96.15	0.188	0.999	13.46	2.068	0.913	3.49	151.8	0.985	61.94	1.324	0.843	
Kinetic coefficients													
Model	Pseudo- first order			Pseudo-second order			Intra-particle			Elovich			
Adsorbate	K_1	R^2	q_e	K_2	R^2		K_{id}	I	R^2	β	R^2		
$Cu^{(II)}$ ions	0.029		0.981	99.01	$5.4*10^{-4}$	0.996		8.22	6.28	0.864	34.37	0.946	

Pseudo-second order:

$$\frac{t}{q_t} = \frac{1}{q_e}t + \frac{1}{k_2 q_e^2} \tag{8}$$

In these equations, k_1 and k_2 are the rate constants, q_e (mg. g^{-1}) is the adsorption capacity, and q_t is the adsorption at time t.

Moreover, the Intra-particle diffusion model was also studied [52] (Eq. 9):

$$q_t = K_{id} t^{\frac{1}{2}} + I \tag{9}$$

K_{id} (mg. g^{-1}. $min^{-1/2}$) stands for the intra-particle diffusion rate constant in this model.

Finally, the Elovich model can be expressed as following [53] (Eq. 10):

$$q_t = \beta Ln(\alpha\beta) + \beta Lnt \tag{10}$$

The adsorption process was completely studied by the intra-particle diffusion model and the Weber-Morris plot (Fig. 7d). The adsorption of $Cu^{(II)}$ ions starts with fast removal of ions followed by a linear plateau. It shows that the adsorption has two separated processes. In the first one, $Cu^{(II)}$ ions were diffusing through the aqueous solution to reach the external surface of THT-TA-CTP, which is mainly a result of electrostatic interactions between the ions and the nitrogen-riched surface, then, at the second one, by the formation of equilibrium, the concentration reached a plateau. [54–56]. A quick comparison between the regression coefficient of Eqs. 7 and 8 shows that the adsorption of $Cu^{(II)}$ ions with THT-TA-CTP obeys the pseudo-second-order equation. The order was independent of $Cu^{(II)}$ ions concentration. Moreover, these results reveal that the adsorption is chemical interaction rather than the physical (Table 1) [57, 58] (Fig. 8).

Comparison with recent studies on cu(II) removal

The performance of THT-TA-CTP was compared to the recent studies in $Cu^{(II)}$ ion removal presented in Table 2. Different materials were studied in the case of copper adsorption, including aminated polyacrylonitrile (entry 1), hierarchical magnetic nanostructures (entry 2), mesoporous alumina (entry 3), nano-composites (entries 4–6), natural polymers (entry 7), hyper cross-linked polymers (entry 8), and microporous polymers (entry 9). However, their results were not satisfactory in the case of time and pH. The presence of nitrogen atoms in the THT-TA-CTP structure and a pincer type interaction to the metal centers made THT-TA an excellent copper adsorbent compared to the materials reported in Table 2.

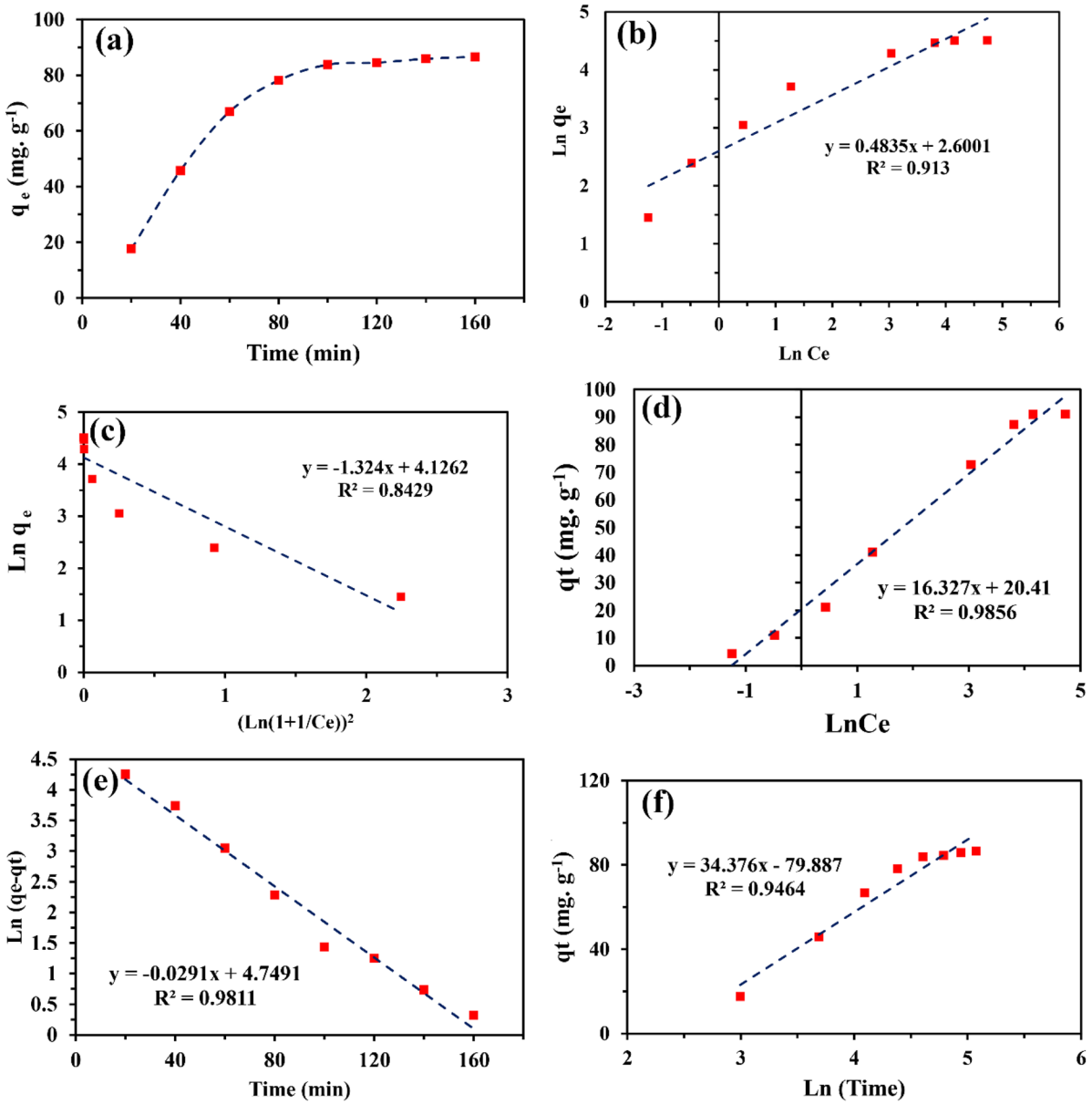

Fig. 8 (**a**) adsorption curve vs. contact time, (**b**) Freundlich, (**c**) Dubinin–Radushkevich, (**d**) Temkin isotherm model, (**e**) pseudo-first-order kinetic model, and (**f**) Elovich kinetic model

Table 2 A comparison of the performance of THT-TA-CTP in the removal of Cu(II) ions

Entry	Adsorbent	C_i[a] (mg. L^{-1})	Time (min)	q_e[b] (mg. g^{-1})	pH	BET surface area (m^2. g^{-1})	Reference
1	APAN[c] nanofibers	100	60	149.8	6	2.8	[59]
2	α-FeOOH@PC	50	540	144.7	7	391.6	[60]
3	protonated mesoporous alumina (PMA)	20	420	8.6	5.8	306	[61]
4	porous geopolymeric sphere	50	2880	52.6	5	53.9	[62]
5	nanocomposite of magnetic hydroxyapatite	10	250	48.8	5	101.2	[63]
6	FCG[d]	100	750	75.4	5	2.53	[64]
7	Cross-linked chitosan beads	5	60	45.94	6	-[e]	[65]
8	melamine-based microporous polymer	10	300	72.9	3.5	548	[66]
9	EDTA functionalized silica	60	20	37.59	5.5	-[e]	[67]
10	THT-TA-CTP	80	240	86.9	7	100.8	This work

[a] initial concentration

[b] adsorption capacity

[c] Aminated polyacrylonitrile

[d] Functionalized chitosan gel

[e] not reported

Conclusions

In summary, THT-TA-CTP was successfully synthesized through a condensation reaction between THT and TA. It was then fully characterized by different techniques such as FE-SEM, XRD, CO_2 Adsorption isotherm, and TGA. The presence of nitrogen atoms in the THT-TA-CTP made it a suitable adsorbent for metal ion removal. The ability of THT-TA-CTP in removing metal ions from aqueous solution was proved using it in $Cu^{(II)}$ ion adsorption with a maximum adsorption capacity of 86.95 mg. g^{-1}. Moreover, `the obtained data reveal that the adsorption isotherm obeys the Langmuir model, and the adsorption kinetics obeys the pseudo-second-order model. By the rapid growth of reticular chemistry and its application in environmental issues, more about covalent organic polymers will be heard in the world of Science. Further studies in preparing new structures with application in water treatment were under investigation by our group.

Acknowledgements We are grateful for the financial support from the Research Council of Isfahan University of Technology (IUT), Isfahan, Iran.

References

1. Bakker K (2012) Water security: research challenges and opportunities. Science 337:914–915
2. Mokhtari N, Dinari M, Rahmanian O (2019) Novel porous organic triazine-based polyimide with high nitrogen levels for highly efficient removal of Ni (II) from aqueous solution. Polym Int 68:1178–1185
3. Srinivas M, Venkata RC, Kakarla RR, Shetti NP, Reddy M, Anjanapura VR (2019) Novel Co and Ni metal nanostructures as efficient photocatalysts for photodegradation of organic dyes. Materials Research Express 6:125502
4. Reddy KR, Karthik K, Prasad SB, Soni SK, Jeong HM, Raghu AV (2016) Enhanced photocatalytic activity of nanostructured titanium dioxide/polyaniline hybrid photocatalysts. Polyhedron 120:169–174
5. Afshari M, Dinari M, Zargoosh K, Moradi H (2020) Novel triazine-based covalent organic framework as a superadsorbent for the removal of mercury (II) from aqueous solutions. Ind Eng Chem Res 59:9116–9126
6. Stanković MN, Krstić NS, Mitrović JZ, Najdanović SM, Petrović MM, Bojić DV, Dimitrijević VD, Bojić AL (2016) Biosorption of Copper (II) ions by methyl-sulfonated Lagenaria vulgaris shell: kinetic, thermodynamic and desorption studies. New J Chem 40:2126–2134
7. Al-Shannag M, Al-Qodah Z, Bani-Melhem K, Qtaishat MR, Alkasrawi M (2015) Heavy metal ions removal from metal plating wastewater using electrocoagulation: Kinetic study and process performance. Chem Eng J 260:749–756
8. Lam B, Déon S, Morin-Crini N, Crini G, Fievet P (2018) Polymer-enhanced ultrafiltration for heavy metal removal: Influence of chitosan and carboxymethyl cellulose on filtration performances. J Clean Prod 171:927–933
9. Li Y, Cui W, Liu L, Zong R, Yao W, Liang Y, Zhu Y (2016) Removal of Cr (VI) by 3D TiO_2-graphene hydrogel via adsorption enriched with photocatalytic reduction. Appl Catal B 199:412–423
10. Peligro FR, Pavlovic I, Rojas R, Barriga C (2016) Removal of heavy metals from simulated wastewater by in situ formation of layered double hydroxides. Chem Eng J 306:1035–1040
11. Tan JZ, Nursam NM, Xia F, Sani M-A, Li W, Wang X, Caruso RA (2017) High-performance coral reef-like carbon nitrides: synthesis and application in photocatalysis and heavy metal ion adsorption. ACS Appl Mater Interfaces 9:4540–4547
12. Xue H, Chen Q, Jiang F, Yuan D, Lv G, Liang L, Liu L, Hong M (2016) A regenerative metal–organic framework for reversible uptake of Cd (ii): from effective adsorption to in situ detection. Chem Sci 7:5983–5988

13. Feng X, Fryxell GE, Wang L-Q, Kim AY, Liu J, Kemner KM (1997) Functionalized monolayers on ordered mesoporous supports. Science 276:923–926
14. Alimohammady M, Jahangiri M, Kiani F, Tahermansouri H (2017) Highly efficient simultaneous adsorption of Cd (II), Hg (II) and As (III) ions from aqueous solutions by modification of graphene oxide with 3-aminopyrazole: central composite design optimization. New J Chem 41:8905–8919
15. Huang N, Zhai L, Xu H, Jiang D (2017) Stable covalent organic frameworks for exceptional mercury removal from aqueous solutions. J Am Chem Soc 139:2428–2434
16. Amarasinghe B, Williams RA (2007) Tea waste as a low cost adsorbent for the removal of Cu and Pb from wastewater. Chem Eng J 132:299–309
17. Bandehali S, Parvizian F, Moghadassi A, Hosseini S (2019) copper and lead ions removal from water by new PEI based NF membrane modified by functionalized POSS nanoparticles. J Polym Res 26:211
18. Li L, Wang Z, Ma P, Bai H, Dong W, Chen M (2015) Preparation of polyvinyl alcohol/chitosan hydrogel compounded with graphene oxide to enhance the adsorption properties for Cu (II) in aqueous solution. J Polym Res 22:150
19. Hao Y-M, Man C, Hu Z-B (2010) Effective removal of Cu (II) ions from aqueous solution by amino-functionalized magnetic nanoparticles. J Hazard Mater 184:392–399
20. Azimi A, Azari A, Rezakazemi M, Ansarpour M (2017) Removal of heavy metals from industrial wastewaters: a review. Chem Bio Eng Reviews 4:37–59
21. Veli S, Alyüz B (2007) Adsorption of Copper and zinc from aqueous solutions by using natural clay. J Hazard Mater 149:226–233
22. Zhao G, Huang X, Tang Z, Huang Q, Niu F, Wang X (2018) Polymer-based nanocomposites for heavy metal ions removal from aqueous solution: a review. Polym Chem 9:3562–3582
23. Uddin MK (2017) A review on the adsorption of heavy metals by clay minerals, with special focus on the past decade. Chem Eng J 308:438–462
24. Lingamdinne LP, Chang Y-Y, Yang J-K, Singh J, Choi E-H, Shiratani M, Koduru JR, Attri P (2017) Biogenic reductive preparation of magnetic inverse spinel iron oxide nanoparticles for the adsorption removal of heavy metals. Chem Eng J 307:74–84
25. Li J, Zheng L, Liu H (2017) A novel carbon aerogel prepared for adsorption of Copper (II) ion in water. J Porous Mater 24:1575–1580
26. Nayak A, Bhushan B, Gupta V, Sharma P (2017) Chemically activated carbon from lignocellulosic wastes for heavy metal wastewater remediation: Effect of activation conditions. J Colloid Interface Sci 493:228–240
27. Peng Y, Huang H, Zhang Y, Kang C, Chen S, Song L, Liu D, Zhong C (2018) A versatile MOF-based trap for heavy metal ion capture and dispersion. Nat Commun 9:1–9
28. Asadi P, Falsafin M, Dinari M (2021) Construction of new covalent organic frameworks with benzimidazole moiety as Fe^{3+} selective fluorescence chemosensors. J Mol Struct 1227:129546
29. Rengaraj A, Haldorai Y, Puthiaraj P, Hwang SK, Ryu T, Shin J, Han Y-K, Ahn W-S, Huh YS (2017) Covalent triazine polymer–Fe_3O_4 nanocomposite for strontium ion removal from seawater. Ind Eng Chem Res 56:4984–4992
30. Fang Q, Wang J, Gu S, Kaspar RB, Zhuang Z, Zheng J, Guo H, Qiu S, Yan Y (2015) 3D porous crystalline polyimide covalent organic frameworks for drug delivery. J Am Chem Soc 137:8352–8355
31. Zhang Y, Riduan SN (2012) Functional porous organic polymers for heterogeneous catalysis. Chem Soc Rev 41:2083–2094
32. Dinari M, Mokhtari N, Taymouri S, Arshadi M (2020) Abbaspourrad, Covalent polybenzimidazole-based triazine frameworks: A robust carrier for non-steroidal anti-inflammatory drugs. Mater Sci Eng C 108:110482
33. Dinari M, Jamshidian F (2021) Preparation of MIL-101-NH_2 MOF/triazine based covalent organic framework hybrid and its application in acid blue 9 removals. Polymer 215:123383
34. Liao Y-T, Ishiguro N, Young AP, Tsung C-K, Wu KC-W (2020) Engineering a homogeneous alloy-oxide interface derived from metal-organic frameworks for selective oxidation of 5-hydroxymethylfurfural to 2, 5-furandicarboxylic acid. Appl Catal B 270:118805
35. Liao Y-T, Matsagar BM, Wu KC-W (2018) Metal–organic framework (MOF)-derived effective solid catalysts for valorization of lignocellulosic biomass. ACS Sustain Chem Eng 6:13628–13643
36. Chueh C-C, Chen C-I, Su Y-A, Konnerth H, Gu Y-J, Kung C-W, Wu KC-W (2019) Harnessing MOF materials in photovoltaic devices: recent advances, challenges, and perspectives. J Mater Chem A 7:17079–17095
37. Konnerth H, Matsagar BM, Chen SS, Prechtl MH, Shieh F-K, Wu KC-W (2020) Metal-organic framework (MOF)-derived catalysts for fine chemical production. Coord Chem Rev 416:213319
38. Lee S-P, Mellon N, Shariff AM, Leveque J-M (2018) Geometry variation in porous covalent triazine polymer (CTP) for CO_2 adsorption. New J Chem 42:15488–15496
39. Nouruzi N, Dinari M, Mokhtari N, Farajzadeh M, Gholipour B, Rostamnia S (2020) Selective catalytic generation of hydrogen over covalent organic polymer supported Pd nanoparticles (COP-Pd). Molecular Catalysis 493:111057
40. Dinari M, Hatami M (2019) Novel N-riched crystalline covalent organic framework as a highly porous adsorbent for effective cadmium removal. J Environ Chem Eng 7:102907
41. Dindar MH, Yaftian MR, Rostamnia S (2015) Potential of functionalized SBA-15 mesoporous materials for decontamination of water solutions from Cr (VI), As (V) and Hg (II) ions. J Environ Chem Eng 3:986–995
42. Raghu A, Gadaginamath G, Aminabhavi TM (2005) Synthesis and characterization of novel polyurethanes based on 1, 3-bis (hydroxymethyl) benzimidazolin-2-one and 1, 3-bis (hydroxymethyl) benzimidazolin-2-thione hard segments. J Appl Polym Sci 98:2236–2244
43. Lim DJ, Marks NA, Rowles MR (2020) Universal Scherrer equation for graphene fragments. Carbon 162:475–480
44. Miranda M, Sasaki J (2018) The limit of application of the Scherrer equation. Acta Crystallographica Section A: Foundations Advances 74:54–65
45. Mokhtari N, Taymouri S, Mirian M, Dinari M (2020) Covalent triazine-based polyimine framework as a biocompatible pH-dependent sustained-release nanocarrier for sorafenib: An in vitro approach. J Mol Liq 297:111898
46. Dombrowski RJ, Lastoskie CM, Hyduke DR (2001) The Horvath–Kawazoe method revisited. Colloids Surf A 187:23–39
47. Dada A, Olalekan A, Olatunya A, Dada O (2012) Langmuir, Freundlich, Temkin and Dubinin–Radushkevich isotherms studies of equilibrium sorption of Zn2 + unto phosphoric acid modified rice husk. IOSR J Appl Chem 3:38–45
48. Abd El-Magied MO, Tolba AA, El-Gendy HS, Zaki SA, Atia AA (2017), Studies on the recovery of Th (IV) ions from nitric acid solutions using amino-magnetic glycidyl methacrylate resins and application to granite leach liquors, Hydrometallurgy, 169: 89–98
49. Lingamdinne LP, Koduru JR, Chang Y-Y, Karri RR (2018) Process optimization and adsorption modeling of Pb (II) on nickel ferrite-reduced graphene oxide nanocomposite. J Mol Liq 250:202–211
50. Jinendra U, Kumar J, Nagabhushana B, Raghu AV, Bilehal D (2019) Facile synthesis of $CoFe_2O_4$ nanoparticles and application in removal of malachite green dye. Green Mater 7:137–142
51. Shahwan T (2015) Lagergren equation: Can maximum loading of sorption replace equilibrium loading? Chem Eng Res Des 96:172–176
52. Ngah WW, Hanafiah M (2008) Adsorption of Copper on rubber (Hevea brasiliensis) leaf powder: Kinetic, equilibrium and thermodynamic studies. Biochem Eng J 39:521–530

53. Abdi J, Vossoughi M, Mahmoodi NM, Alemzadeh I (2017) Synthesis of metal-organic framework hybrid nanocomposites based on GO and CNT with high adsorption capacity for dye removal. Chem Eng J 326:1145–1158
54. Ahsaine HA, Zbair M, Anfar Z, Naciri Y, Alem NE, Ezahri M (2018) Cationic dyes adsorption onto high surface area 'almond shell'activated carbon: kinetics, equilibrium isotherms and surface statistical modeling. Materials Today Chemistry 8:121–132
55. Ahsaine HA, Zbair M, Haouti RE (2017) Mesoporous treated sewage sludge as outstanding low-cost adsorbent for cadmium removal. Desalin Water Treat 85:330–338
56. Aoudj S, Khelifa A, Drouiche N, Belkada R, Miroud D (2015) Simultaneous removal of chromium (VI) and fluoride by electrocoagulation–electroflotation: application of a hybrid Fe-Al anode. Chem Eng J 267:153–162
57. Ahmad M, Manzoor K, Ahmad S, Ikram S (2018) Preparation, kinetics, thermodynamics, and mechanism evaluation of thiosemicarbazide modified green carboxymethyl cellulose as an efficient Cu (II) adsorbent. J Chem Eng Data 63:1905–1916
58. Nabi SA, Shahadat M, Shalla AH, Khan AM (2011) Removal of heavy metals from synthetic mixture as well as pharmaceutical sample via cation exchange resin modified with rhodamine B: its thermodynamic and kinetic studies. CLEAN–Soil Air Water 39:1120–1128
59. Chen C, Li F, Guo Z, Qu X, Wang J, Zhang J (2019) Preparation and performance of aminated polyacrylonitrile nanofibers for highly efficient copper ion removal. Colloids Surf A 568:334–344
60. Yang F, Zhang S, Li H, Li S, Cheng K, Li J-S, Tsang DC (2018) Corn straw-derived biochar impregnated with α-FeOOH nanorods for highly effective copper removal. Chem Eng J 348:191–201
61. Rengaraj S, Kim Y, Joo CK, Yi J (2004) Removal of Copper from aqueous solution by aminated and protonated mesoporous aluminas: kinetics and equilibrium. J Colloid Interface Sci 273:14–21
62. Ge Y, Cui X, Kong Y, Li Z, He Y, Zhou Q (2015) Porous geopolymeric spheres for removal of Cu (II) from aqueous solution: synthesis and evaluation. J Hazard Mater 283:244–251
63. Thanh DN, Novák P, Vejpravova J, Vu HN, Lederer J, Munshi T (2018) Removal of Copper and nickel from water using nanocomposite of magnetic hydroxyapatite nanorods. J Magn Magn Mater 456:451–460
64. Yang Z, Chai Y, Zeng L, Gao Z, Zhang J, Ji H (2019), Efficient Removal of Copper Ion from Wastewater Using a Stable Chitosan Gel Material, Molecules, 24: 4205
65. Ngah WW, Endud C, Mayanar R (2002) Removal of Copper (II) ions from aqueous solution onto chitosan and cross-linked chitosan beads. React Funct Polym 50:181–190
66. Taskin OS, Ersoy N, Aksu A, Kiskan B, Balkis N, Yagci Y (2016) Melamine-based microporous polymer for highly efficient removal of Copper (II) from aqueous solution. Polym Int 65:439–445
67. Melo DQ, Neto VO, Oliveira JT, Barros AL, Gomes EC, Raulino GS, Longuinotti E, Nascimento RF (2013) Adsorption equilibria of Cu^{2+}, Zn^{2+}, and Cd^{2+} on EDTA-functionalized silica spheres. J Chem Eng Data 58:798–806